CHAPTER 4 STATISTICAL CONVERGENCE

4.1 Forces and Moment and Motions Data

Single records of forces and moment and motions data for static and dynamic PMM tests are analyzed and statistical convergence of data are estimated. Herein single record implies a set of data acquired during individual carriage runs. Analysis begins with classifications of data into either deterministic or random data where further into either periodic or transient for the former category and into either stationary or non-stationary for the latter category. The term 'deterministic' implies that data can be described explicitly by a mathematical relationship, on the other hand, the term 'random' means that data cannot be described by explicit mathematical relationship, instead, by means of probability statements and/or statistical averages (Bendat 1966, pp. 2). A practical decision whether or not data are deterministic or random, as per Bendat, is usually based on the ability to reproduce the data by controlled experiments. Accordingly, herein for PMM applications, only the time mean values of static drift test data and the harmonics of dynamic tests data are classified as deterministic, while all the other components of data including transient are considered as random. Once deterministic part of data is decided, the stationarity of the random part of data is of interest since only stationary data are guaranteed to converge. Stationarity of data is tested by using nonparametric (distribution-free) statistical procedures such as the 'run test' and 'trend test'. Next, statistical convergence of the time mean values of static drift test data is estimated based on the convergence of confidence interval of the mean values. Typically, data samples containing narrow-banded sinusoid components or transient components may not be distributed normally, thus confidence interval is estimated using the Tchebycheff inequality for unknown distributions rather than the Student-t for normal distributions. Statistical convergence, however, may not be applicable for dynamic tests data since usually two or three periods of data are available due to limited length of IIHR towing tank facility.

4.1.1 Time History of data

Typical examples of time history and Fast Fourier Transform (FFT) of data are shown in Fig. 4-1 for static drift test. Data includes carriage speed (U_C), drift angle (β), forces (F_x, F_y), moment (M_z), and motions (z_{mm}, θ, ϕ). Of those variables, U_C, β, and ϕ are the controlled (input) parameters set at the desired values 1.531 m/s, -10°, and 0°, respectively, whereas F_x, F_y, M_z, z_{mm}, and θ are the results (output) of the test. Data are sampled at a rate of 100Hz (i.e. $\Delta t = 0.01$ sec) for a time-period of $T = 20$ sec corresponding to $U_C \cdot T/L \approx 10$ where $L = 3.148$ m is the model length. Data acquisition commences after carriage acceleration and U_C nearly constant, which takes about 3 ~ 4 L. For FFT, total $N = 1{,}024$ data are selected from the time history of each variable, between t = 5 ~ 15 sec, which gives a frequency step $\Delta f = 1/N \cdot \Delta t \approx 0.1$ Hz in the FFT. Time histories are shown for one case out of 12 repeat tests at the same conditions, whereas the FFT results are shown for all the 12 cases emphasizing the repeatability of measurement. FFT data as well include two different β cases (0° and -20°) for possible hydrodynamic effects on the results, which may or may not increase with β, particularly in the frequency domain.

For U_C shown in Fig. 4-1 (a), time history exhibits random fluctuations of which root-mean-square (rms) value is 0.008 m/s (about 0.5% of the mean $U_C = 1.514$ m/s). Dominant frequency of the random fluctuation is between 1 ~ 2.5 Hz from the FFT that as well reveals the underlying long-period oscillations of data with frequencies between 0.1 ~ 0.6 Hz, otherwise seemingly white noise. Drift angle β shown in Fig. 4-1 (b) also exhibits long-period oscillations with an amplitude 0.06° (about 0.6% of the mean $\beta = -10.1°$) and dominant frequency between 0.1 – 0.3 Hz from the FFT otherwise white noise. Roll angle ϕ shown in Fig. 4-1 (c) is almost random fluctuation with an rms value 0.02° (about 36% of the mean $\phi = -0.05°$) and dominant frequencies 1.2 and 2 Hz maybe coherent with those for U_C. Possible sources for long period oscillations of U_C can be carriage speed control-loop feedback or non-perfectly straight rail alignments, and the sources for random fluctuations of U_C can be mechanical vibrations due to the irregular

surfaces of the carriage wheels and/or rails. Which may cause the long period oscillations and/or high frequency fluctuations in β and ϕ, too. Deviations of the mean values of those variables from the initial set-up values, -10° and 0°, respectively, can be attributed in part to the model mount flexibility and in part to model asymmetry. Note that although not shown, mean ϕ value grows with β, -0.004° and -0.07° at β = 0° and -20°, respectively.

Responses in forces and moment and motions to the aforementioned input parameters, U_C, β, and ϕ, are shown in Fig. 4-1 (d) – (h) for F_x, F_y, M_z, z_{mm}, and θ. From time histories, F_x, F_y, and M_z are random fluctuations with rms values 3.4 N, 3.3 N, and 3.4 Nm (32%, 12%, and 8% of the mean values -10.7 N, -28.1 N, and -43.4 Nm), respectively. From FFT, those random fluctuations are narrow banded, in general between 2 – 10 Hz with sharp peaks typically near at 3, 4, 5, and 10 Hz due mainly to mechanical vibrations as will be identified latter. On the other hand, heave and pitch motions z_{mm} and θ time histories shown in Fig. 4-1 (g) and (h) are random fluctuations superposed on apparently transient oscillations. The random fluctuations are with rms values 0.5 mm and 0.01° (5% of mean z_{mm} = 8.9 mm and 9% of mean θ = -0.153°) respectively. The transient oscillations are typically damped oscillations that can be written in a mathematic form as $Ae^{-at}\cos(2\pi f_{tr}t)$. The oscillation amplitude A is 1.13 mm and 0.09° (13% of mean z_{mm} and 59% of mean θ) respectively, however, subject to random depending on the time point where data sampling commences. The damping coefficient a = 0.08 sec^{-1} and the oscillation frequency f_{tr} = 0.255 Hz are the same for both z_{mm} and θ. Although not shown, in general A increases with β whereas a and f_{tr} are nearly constant. Those transient oscillations are due to start-up transient such that f_{tr} is far from z_{mm} and θ natural frequency $f_3 = f_5$ = 1.2 Hz estimated from hydrostatic restoring forces (Irvine et al. 2008). The heave natural frequency f_3 is clearly seen from the FFT for z_{mm} shown in Fig. 4-1 (g) while the pitch natural frequency f_5 is less distinctive from the FFT for θ shown in Fig. 4-1 (h). Note that it is not clear if the similar or same peak frequencies of U_C, i.e. near 0.2

Hz and 1.2 Hz form Fig. 4-1 (a), are coincidence or there may exist interactions between towing speed and model motions.

Dynamic test time history and FFT are shown in Fig. 4-2 similarly as for static drift test. Shown at the left column are the time histories of pure sway test data for one case out of 12 repeat tests at β_{max} = 10° condition. Carriage speed U_C, sway trajectory y, and heading angle ψ shown in (a) – (c) are the controlled (input) parameters for pure sway test. The overall trend of U_C (set at 1.531 m/s) is similar as for static drift test discussed previously. Sway trajectory $y = A \sin(2\pi f_{\mathrm{PMM}} t)$ is a forced sinusoidal oscillation with A = 0.317 m (about 0.1 L) and f_{PMM} = 0.134 Hz. Heading angle ψ is set at zero but exhibits an oscillation with amplitude 0.06° and almost out of phase with y. Although not shown, roll angle ϕ is also set at zero and shows an oscillation with amplitude 0.1° and out of phase with y. Forces and moment F_x, F_y, and M_z in (d) – (f) are random fluctuations with rms values 4.0 N, 4.7 N, and 2.3 Nm (54%, 4%, and 3% of the dynamic range 7.4 N, 114.4 N, and 92.7 Nm) respectively, over-riding the harmonic oscillations with f_{PMM} as the fundamental frequency. Heave z_{mm} and pitch θ motions in (g) and (h) are mixtures of harmonic oscillation, transient oscillation, and random fluctuations. Harmonic oscillations are with f_{PMM} as the fundamental frequency. Transient oscillations may be similar as for static drift test, however, it is difficult to identify them from the signal as the transient oscillation frequency f_{tr} = 0.255 Hz is close to the dominant harmonic (the 2nd order harmonic) frequency $2f_{PMM}$ = 0.268 Hz for both variables. Random fluctuations are with rms values 0.4 mm and 0.015° (7% of mean z_{mm} = 5.6 mm and 10% of mean θ = -0.164°) respectively. For dynamic test data, the harmonic oscillation component of each variable data is classified as deterministic and other components including transient oscillations and random fluctuations as random data, designated with a '*' symbol such that

$$x^* = x(t) - x_{\mathrm{FS}}(t) \tag{4.1}$$

where x can be any dynamic test variable (except for U_C) and x_{FS} is the harmonic component of x evaluated using a Fourier Series (FS) expansion of x with f_{PMM} as the fundamental frequency. Note that U_C is independent of f_{PMM} and not expanded with FS. Note also for z_{mm} and θ that x_{FS} can include the transient oscillation component of the variable data when $f_{tr} \approx n \cdot f_{PMM}$ for any integer number of n. At the right column of Fig. 4-2, shown are the FFT results of x^* for all types of dynamic test including pure sway, pure yaw, and yaw and drift tests, which are the UA cases of each test with 12 repeat tests. In general the FFT results for each type of dynamic tests are similar each other, and as well similar with those for static drift test shown in Fig. 4-1. For U_C in (a), same discussions can be make as for static drift test. For y and ψ in (b) and (c), two peak frequencies in the FFT are observed near at $3f_{PMM}$ and $5f_{PMM}$ but with very small amplitudes, usually much less than 0.1% of the range of the variables. For F_x, F_y, and M_z in (d) – (f), peak frequencies are usually near 3, 4, 5, 7, and 10 Hz similarly as static drift data. FFT's for z_{mm} and θ shown in (g) and (h) are almost same as those for static drift except for relatively smaller amplitudes at the frequency range between 0.1 – 0.3 Hz as $f_{tr} \approx 2f_{PMM}$ for all cases.

A separate set of tests were carried out identifying the sources of peak frequencies of the forces and moment data. Test was done first without the model and only the load-cell was installed to the PMM carriage that is connect to the driving carriage. Tests included total 11 cases arranged into five groups (A, B, C, D, and E) as summarized in Table 4-1. Model was not installed for Groups A, B, C, and D whereas installed for Group E but in air to avoid any possible hydrodynamic effects. Tests were stationary in surge direction for Groups A, B, and C with $U_C = 0$ whereas in towing motion for Groups D and E with $U_C = 1.531$ m/s (with two repeat tests for Group E). The PMM motor was turned on for all test groups rotating with one of the three cyclic frequencies $f_e = 0.01$, 0.96, or 0.134 Hz to excite the load-cell. Group A emphasizes the natural frequencies of the PMM system including the load-cell by minimizing any possible external noise sources but f_e. Groups B and C are intended to include the effects of mechanical vibra-

tions from the Scotch Yoke system for PMM. Groups D and E are to include mechanical vibrations of the PMM system from such as non-perfectly regular surfaces of the rails and/or wheels of carriages. The FFT results of the test are shown in Fig. 4-3, for which the harmonics of the excitation frequency f_e up to the 6^{th} order were filtered out from the signals using the equation (4.1). From Fig. 4-3 (a) – (f), the responses are at very specific frequencies near 5 and 7 Hz. From Fig. 4-3 (g) – (l), as the carriages are running, many of peak frequencies appear roughly between 2 – 10 Hz with sharp peaks near at 3, 4, 5, 7, and 10 Hz. Consequently, test results suggest that the sources of the 5 and 7Hz are the natural frequencies of the load-cell, the PMM carriage, or combined, and the sources of the 3, 4, and 10 Hz are from the mechanical vibration. However, more study is needed to determine whether a portion may be due to hydrodynamic sources such as flow turbulence, flow separation instabilities, and/or, vortex breakdown.

4.1.2 Stationarity Test

The time history data are tested for stationarity by using the two non-parametric statistical procedures known as 'Run test' and 'Trend test' (Bendat 1966, pp. 219 - 223). Four important assumptions made for the stationarity tests are: 1) If the data of interest are stationary, then the statistical properties computed for each sequence of short time intervals will not vary significantly from on time interval to the next; 2) Verification of weak stationarity (time invariance of the mean value and autocorrelation function) will be acceptable; 3) The sample record of the data to be investigated is very long compared to the random fluctuations of the data time history; 4) If the mean square value (or variance) of the data of interest is stationary, then the autocorrelation function for the data is also stationary. Some important features of the non-parametric (or distribution-free) procedures which do not assume a specific distribution for the random data are: 1) The frequency bandwidth of the data is not required; 2) The exact averaging time used to measure the mean and mean square values is not required; 3) It is not necessary for the data to

be completely random. Two non-parametric procedures 'Run test' and 'Trend test' are briefly summarized from Bendat (1966, pp. 156 – 159) as follows.

Run test: Consider a sequence of N observations of a random variable x where each observation is classified into one of two mutually exclusive categories, which may be identified simply by plus (+) or minus (-). The simplest example would be a sequence measured values x_i, i = 1, 2, 3, …, N, with a mean value $\bar{x}$, where each observation is $x_i \geq \bar{x}$ (+) or $x_i < \bar{x}$ (–). A run is defined as a sequence of identical observations that are followed or preceded by a different observation or no observation at all. For example; ++ (1), – (2), ++ (3), – (4), +++ (5), – (6), + (7), – – (8), + (9), – – (10), + (11), – – – (12). In this example there are r = 12 runs in the sequence of N = 20 observations. The number of runs which occur in a sequence of observations gives an indication as to whether or not results are independent random observations of the same random variable. Specifically, if a sequence of N observations are independent observations of the same random variable, that is, the probability of a (+) or (-) result does not change from one observation to the next, then the sampling distribution for the number of runs in the sequence is a random variable r with a mean value and variance as follows.

$$\mu_r = \frac{N}{2} + 1 \qquad (4.2)$$

$$\sigma_r^2 = \frac{N(N-2)}{4(N-1)} \qquad (4.3)$$

Trend test: Consider a sequence of N observations of a random variable x, where the observations are denoted by x_i, i = 1, 2, 3, …, N. Now, count the number of times that $x_i > x_j$ for i < j. Each such inequality is called a reverse arrangement. The total number of reverse arrangements is denoted by A. A general definition for A is as follows. From the set of observations $x_1, x_2, \ldots, x_N$, define

$$h_{ij} = \begin{cases} 1 & if\ xi > xj \\ 0 & otherwise \end{cases} \qquad (4.4)$$

Then

$$A = \sum_{i=1}^{N-1} A_i \qquad (4.5)$$

where

$$A_i = \sum_{j=i+1}^{N} h_{ij} \qquad (4.6)$$

If the sequence of N observations are independent observations of the same random variable, then the number of reverse arrangements is a random variable A with a mean and variance as follows.

$$\mu_A = \frac{N(N-1)}{4} \qquad (4.7)$$

$$\sigma_A^2 = \frac{N(2N+5)(N-1)}{72} \qquad (4.8)$$

In general, the trend test is more powerful than the run test for detecting monotonic trends in a sequence of observations, however, not powerful for detecting fluctuating trends.

For stationarity tests the time histories of static drift test and pure sway test data shown in Figs. 4-1 and 4-2 are divided into $N = 20$ equal time intervals with an interval size of 100 data per each interval (corresponding to 1 sec), where the data in each interval may be considered independent. Note for pure sway data (and for all dynamic tests data) that stationarity tests are applied only for the random component of data x^* defined in equation (4.1). Once proved the stationarity of its random part, then the dynamic data is referred herein as stationary. Next, a mean value ($\bar{x}_1, \bar{x}_2, \bar{x}_3, \ldots, \bar{x}_N$) and mean square value ($\overline{x_1^2}, \overline{x_2^2}, \overline{x_3^2}, \ldots, \overline{x_N^2}$) for each interval are computed and aligned in time sequence as shown in Fig. 4-4. It is hypothesized that the sequence of $\bar{x}$ and the sequence of $\overline{x^2}$ are each independent sample values of a random variable with a true mean value and mean square value, respectively. If this hypothesis is true, the variations in the sequence of sampled values will be random and display no trends. Hence, the number of runs in the sequence will be as expected for a sequence of independent random observations of the random variable. Moreover, the number of reverse arrangements in the sequence will be as expected for a sequence of independent random observations of the same variable. If the number of runs or reverse arrangements is significantly different from the expected number, the hypothesis of stationarity would be rejected.

Run and Trend tests results are presented in Table 4-2 for static drift and pure sway tests data, respectively. Both tests were performed at the 5% level of significance. Then, the acceptance region[8] is $6 \le r \le 15$ for the run test and $64 \le A \le 125$ for the trend

[8] The acceptance region can be read from a statistics tables (e.g. Bendat 1966, pp. 170 – 171) or calculated as follows.

test, respectively, for $N = 20$. From Table 4-2, r and A values of the mean square $\overline{x^2}$ for all variables are within the acceptance regions of run test and trend test, indicating there is no evidence of an underlying trend. However, r and A values of the mean $\bar{x}$ value for some variables are outside the acceptance regions, indicating possible non-stationarity of those variables. For static drift data, only β fails the run test ($r = 5$ for $\bar{x}$) whereas U_C, ϕ, and F_y fail the trend test ($A = 145$, 127, and 133 for $\bar{x}$, respectively). For pure sway data, F_x, F_y, and z_{mm} fail the run test ($r = 16$, 5, and 4 for $\bar{x}$, respectively) whereas U_C, y, and z_{mm} fail the trend test ($A = 136$, 126, and 129 for $\bar{x}$, respectively). When the tests are performed for collections of data from the 12 repeat tests, however, the average r and A values show that U_C, β, and ϕ fail the tests and the other variables F_x, F_y, M_z, z_{mm}, and θ are all stationary in an average sense. Nonetheless, the average r and A values for β ($r = 5$) and ϕ ($A = 130$, 126) are not significantly different from the acceptance regions such that can be considered as accepted if lower the level of significance of test to 1% of which acceptance region is $5 \le r \le 16$ for the run test and $59 \le A \le 130$ for the trend test, respectively. U_C fails both the run test ($r = 5$) and the trend test ($A = 143$, 140) revealing a strong evidence of an underlying trend. The underlying trend in U_C can be easily seen from Fig. 10 (a) where a step-wise decrease in the interval mean value of U_C is observed near at the 12th interval and as well from Figs. 4-1 (a) and 4-2 (a) where apparent decrease of U_C in the time histories neat at $t = 12$ sec. This decrease of U_C is considered as due to the lack in electric power for driving two carriages, the main driving carriage and the PMM carriage, at the same time. However, the amount of change of U_C is fairly

---

$(\mu_{r,A} + z_{1-\alpha/2} \cdot \sigma_{r,A}) \le r, A \le (\mu_{r,A} + z_{\alpha/2} \cdot \sigma_{r,A})$

where $\alpha = 0.05$ and $z_{\alpha/2} = -z_{1-\alpha/2} = 1.96$ for 5% level of significance and μ_r, σ_r, μ_A, σ_A are given in equations (4.2), (4.3), (4.7), (4.8), respectively. Note that the limit value of the acceptance region should be rounded down to an integer number.

small (usually 0.6 ~ 0.7% of mean U_C) such that the stationarity of other variables is not affected significantly or at least not noticeable.

4.1.3 Statistical Convergence

Convergence of a random data being measured as time history can be defined such that the result of data, e.g. the mean value, does not change as acquiring more and more data. The Law of Large Numbers (e.g., Feller, 1968) guarantees that for any random data, x, the sample mean converges to an expected value (the true mean of x) when an infinite number of data is available. However, the number of data collectable from practical situations is in general limited to a finite number N, hence the extent of difference between the true mean μ_x and the sample mean $\bar{x}$ of the N data is of interest. Herein, the difference is estimated using a statistical concept of confidence interval for $\bar{x}$ with a certain probability. When the limit of interval, d, is smaller than a predetermined (or desired) value as increasing the sample size N, then the variable x is said to be 'statistically converged' and d is defined as the 'statistical convergence error' in $\bar{x}$.

Confidence interval of $\bar{x}$ is usually estimated by assuming a normal distribution of the random variable x and subsequently by assuming the Student-t distribution of $\bar{x}$, which is the underlying basic concept of typical uncertainty analysis procedures estimating the precision limit. The normal distribution assumption is justified by virtue of the central limit theorem for the precision limit of which random variable is the mean of each x time histories from a collection (ensemble) of repeated tests at the same conditions. In general, however, a normal distribution assumption is not justified for a single record of time history data that may contain narrow band sinusoid components and/or transient components as discussed previously for time histories of the PMM test data. In such a case a more generous and robust inequality, the Tchebycheff inequality, may be used estimating the confidence interval for any variable x without knowing the exact distribu-

tion. The Tchebycheff inequality can be written in probability statement as follows (Bendat 1966, pp. 62).

$$\text{Prob}\left[|\bar{x} - \mu_x| \leq c \cdot \frac{\sigma_x}{\sqrt{N}}\right] \geq 1 - \frac{1}{c^2} \tag{4.9}$$

where μ_x and σ_x is the true mean and standard deviation of x, respectively, $\bar{x}$ is the sample mean and N is the sample size of the x time history, and c can be any positive real number. The meaning of Tchebycheff inequality is that the probability for the true mean to fall within an interval $(\bar{x} - d, \bar{x} + d)$ where $d = c \cdot \sigma_x/\sqrt{N}$ is larger than $p = 1 - 1/c^2$ regardless of underlying distribution of x. In other words, the absolute difference between the true mean and the sample mean would be smaller than d with a confidence of $100p$ percent, for example, 95% for $c = 4.5$. A difficulty in applications of the inequality (9), however, arise from the fact that the true standard deviation σ_x value is unknown for the most of practical cases. Thus, herein the sample standard deviation s_x is used as a best estimator of σ_x for practical application purposes such that an approximate confidence interval $\hat{d}$ and the statistical convergence error $E_{sc}(\%)$ are defined as follows.

$$\hat{d} \equiv c \cdot \frac{s_x}{\sqrt{N}} \tag{4.10}$$

$$E_{sc}(\%) \equiv \frac{\hat{d}}{\bar{x}} = \frac{c}{\sqrt{N}} \cdot \frac{s_x}{\bar{x}} \times 100 \tag{4.11}$$

where N is the sample size, $\bar{x}$ and s_x are the sample mean and standard deviation, respectively, and $c = 4.5$ for a 95% confidence. Note that $\hat{d}$ is equivalent to the confidence interval for a normal distribution when $N > 10$ and $c = t = 2.0$ in (10), which has the same 95% confidence level.

Knowing the normality of data is important to estimate the convergence as it allows one to use the Student t instead of the c in (11) along with the justification for the use of sample standard deviation. Normality of data is tested using the chi-square good-

ness-of-fit test (Bendat 1966, pp. 146). For the test, data are grouped into K class intervals determined by using the 'minimum optimum number of class' for a sample size of N (Williams, C.A., Jr., 1950), which gives

$$\mathrm{X}^2 = \sum_{i=1}^{K} \frac{(f_i - F_i)^2}{F_i} \tag{4.12}$$

where f_i and F_i are the observed frequency and the expected frequency in the ith class interval, respectively. The acceptance region for a hypothesis that the data of interest is normal is

$$\mathrm{X}^2 \leq \chi^2_{n;\alpha} \tag{4.13}$$

where $\chi^2_{n;\alpha}$ is the χ^2 value for a degree of freedom $n = K - 3$ and for an α level of significance of the test. If the sample value of X^2 is greater than $\chi^2_{n;\alpha}$, the normality hypothesis is rejected.

In Fig. 4-5, shown are the sample distributions of the static drift U_C, β, ϕ, F_x, F_y, M_z, z_{mm}, and θ data collected from 12 repeat tests (designated with symbols 1 ~ 9, A, B, and C in the figure) with compared to theoretical standard normal distribution. The $\overline{\mathrm{X}^2}$ values shown in the figure are the average X^2 values tested for each of the 12 repeat cases. An interval size $K = 39$ is used for the sample size $N = 2{,}000$ and the chi-square tests are done at the 5% level of significance ($\alpha = 0.05$), which gives $\chi^2_{36;0.05} = 51.0$. Test result is fail for all variables as X^2 values are larger than $\chi^2_{36;0.05}$, whereas relatively not significantly for F_x, F_y ,and M_z ($\overline{\mathrm{X}^2} = 60.5$, 72.1, and 119.8, respectively) showing their probability density functions (pdf's) close to a normal distribution in Fig. 4-5 (d) – (f). The $\overline{\mathrm{X}^2}$ values for z_{mm}, ϕ, and θ (121.5, 139.0, and 145.5,) are relatively moderately and those for U_C, and β (471.8 and 1737.3) are significantly larger than $\chi^2_{36;0.05}$, respectively, showing moderate and significant discrepancies of pdf from a normal distribution as

shown in Fig. 4-5 (g), (c), (h), respectively and in Fig. 4-5 (a) and (b), respectively, respectively.

Running mean $\bar{x}(N)$ and standard deviation $s_x(N)$ values are shown in Fig. 4-6 (left column) for static drift test data $x = U_C$, β, ϕ, F_x, F_y, M_z, z_{mm}, and θ of which time histories are shown in Fig. 4-1. The $\bar{x}(N)$ and $s_x(N)$ are the sample mean and sample standard deviation values for a subset of data with a sample size N increasing from 1 to 2,000 (in time-wise from $t = 0.01$ to 20.0 sec) by continuously adding more and more data to the sample. In Fig. 4-6, the $\bar{x}(N)$ and $s_x(N)$ are normalized with their final values, i.e. values at $N = 2{,}000$, designated as $\bar{x}^*(N)$ and $s_x^*(N)$, respectively, emphasizing the convergence of those values. In general, both $\bar{x}^*(N)$ and $s_x^*(N)$ at first oscillate and then converge to their final values, a unity, as N increasing. The statistical convergence error $E_{sc}(\%)$ values of those variables are as well shown in Fig. 4-6 (right column), evaluated as per equation (4-11) using the $\bar{x}(N)$ and $s_x(N)$ values at each N. Shown in the figure are the $E_{sc}(\%)$ values using two c values, $c = 2.0$ and $c = 4.5$, providing a 75% and a 95% confidence in $\hat{d}$, respectively, from the Tchebycheff inequality. Summarized in Table 4-3 are the confidence interval $(\bar{x}^*(N) - \hat{d}^*, \bar{x}^*(N) + \hat{d}^*)$ values at $N = 1{,}000$, where $\hat{d}^*$ is the normalized $\hat{d}$ value similarly as for $\bar{x}^*(N)$, and the $E_{sc}(\%)$ values at $N = 2{,}000$, which are the average values of 12 repeat tests. Discussions for the results follow.

From the left column of Fig. 4-6, the convergence of $\bar{x}^*(N)$ can be categorized into three types according to the trend of $s_x^*(N)$ with N after the initial oscillation phase; almost const (Type I), decreasing (Type II), or increasing (Type III) with N, respectively. Variables F_x, F_y, and M_z shown in Fig. 4-6 (d), (e), and (f) correspond to Type I, of which sample distributions were close to a normal distribution as discussed previously. Confidence interval of those variables evaluated at $N = 1{,}000$ (shown as dashed lines, green for $c = 2.0$ and red for $c = 4.5$) well include the future $\bar{x}^*(N)$ values up to $N = 2{,}000$ even with $c = 2.0$. Variables z_{mm} and θ shown in Fig. 4-6 (g) and (h) correspond to Type II, which are the variables contain transient components in their data time histories. Con-

fidence interval of those variables evaluated at N = 1,000 for the c = 4.5 case contains the future $\bar{x}^*(N)$ but not for the c = 2.0 case. Variables U_C, β, and ϕ shown in Fig. 4-6 (a), (b), and (c) correspond to Type III, which are the variables of which dominant frequencies in data time history are low near at 0.1 ~ 0.2 Hz. Confidence interval of those variables evaluated at N = 1,000 does not contain future $\bar{x}^*(N)$ even for the c = 4.5 case. For the Type I or II data, the sample standard deviation s_x is either constant or decreasing as the sample size N is increasing. The true standard deviation σ_x is expected to be similar with or smaller than the sample standard deviation, which may justify the use of s_x in equation (4-10) instead of σ_x. For a pure sine wave, for example, of which $\sigma_x = 1/\sqrt{2}$ is known, the ratio $s_x/\sigma_x \approx 1.04$ after about one cycle and $s_x/\sigma_x < 1.01$ after about four cycles. For the Type III data, however, the use of s_x instead of σ_x is not justified, possibly the data sampling time might not be long enough to include more than four cycles of the long period (low frequency) oscillation of data.

From the right column of Fig. 4-6, the statistical convergence error E_{sc}(%) typically decrease with N either fast or gradually. The rate of decrease of E_{sc}(%) with N seem to be with regardless of the type of convergence discussed above, rather related to the ratio $s_x/\bar{x}$ value summarized Table 4-3. For U_C and β shown in Fig. 4-6 (a) and (b), the ratio $s_x/\bar{x}$ = 0.006 and 0.003, respectively, is so small that E_{sc}(%) becomes immediately smaller than 0.2% and 0.1%, respectively. For F_y, M_z, and z_{mm} shown in Fig. 4-6 (e), (f), and (g), the ratio $s_x/\bar{x}$ = 0.11, 0.08, and 0.07, respectively, is moderate small and *Esc*(%) value becomes smaller than 1% after $N \approx 400$ ($U_C \cdot t/L \approx 2$) for c = 2.0 and after $N \approx 1{,}400$ ($U_C \cdot t/L \approx 7$) for c = 4.5 except for F_y for the latter case. For ϕ, F_x, and θ shown in Fig. 4-6 (c), (d), and (h), the ratio $s_x/\bar{x}$ = 0.36, 0.30, and 0.25, respectively, is relatively larger than other variables and E_{sc}(%) value is larger than 1% even at N = 2,000 for both c = 2.0 and c = 4.5 cases.

Consequently, three factors play important roles for statistical convergence of data, which are the normality, the trend of sample standard deviation, and the ratio of stan-

dard deviation to the mean value of the data, respectively. When data are normal or nearly normal (such as F_x, F_y, or M_z), the statistical convergence error E_{sc}(%) can be evaluated using the confidence interval d evaluated with the Student t = 2.0 for a 95% confidence level, similarly as for typical uncertainty analysis procedures estimating the precision limit, which is equivalent to using $\hat{d}$ in equation (4-10) with c = 2.0. However, when data are not normal the used of Student t may underestimate the convergence error more than two times at the same level of confidence (e.g. for 95%, c/t = 4.5/2.0 = 2.25), and the distribution-free Tchebycheff inequality should be used estimating the confidence interval. More specifically, when data are not normal but the sample standard deviation s_x is almost constant or decreasing with N (such as z_{mm} or θ) the use of s_x in the Tchebycheff inequality is justified and the E_{sc}(%) can be estimated using the confidence interval $\hat{d}$ in equation (4-10) with c = 4.5 for a 95% confidence level. When data are not normal and the s_x is increasing with N (such as U_C, β, or ϕ), however, the used of s_x in the Tchebycheff inequality is not justified and the E_{sc}(%) may not be estimated properly. Lastly, the statistical convergence of data is also dependent on the ratio $s_x/\bar{x}$; data converge fast when the ratio $s_x/\bar{x}$ is small (such as U_C or β), gradually for moderate $s_x/\bar{x}$ values (such as F_y, M_z, or z_{mm}), and rather slowly for larger $s_x/\bar{x}$ values (such as ϕ, F_x, or θ), respectively.

Table 4-1 Noise Test Conditions.

Group	Model	U_C (m/s)	$2S_{mm}$ (mm)	ψ_{max} (°)	f_e (Hz)
A	Not Installed	0	0	0	0.010, 0.096, 0.134
B	Not Installed	0	317	0	0.010, 0.096, 0.134
C	Not Installed	0	318	14.2	0.010, 0.096, 0.134
D	Not Installed	1.531	317	0	0.134
E	Installed (in air)	1.531	327	10.2	0.134

Table 4-2 Tests for Stationarity.

	Run Test, r †($6 \le r \le 15$ for $N = 20$)				Trend Test, A †($64 \le A \le 125$ for $N = 20$)			
	Static drift		Pure sway		Static drift		Pure sway	
Var.	$\bar{x}$	$\overline{x^2}$	$\bar{x}$	$\overline{x^2}$	$\bar{x}$	$\overline{x^2}$	$\bar{x}$	$\overline{x^2}$
U_C	6 (5)	11 (10)	6 (5)	12 (12)	145 (143)	104 (104)	136 (140)	116 (104)
β or y	5 (5)	12(11)	9 (9)	6 (8)	82(82)	71(89)	126 (105)	101 (95)
ϕ	7 (6)	9 (10)	9 (7)	6 (9)	127 (130)	78 (96)	121 (126)	68 (90)
F_x	12 (12)	10 (10)	16 (13)	10 (11)	108 (103)	100 (100)	92 (102)	76 (92)
F_y	8 (8)	12 (9)	5 (7)	6 (9)	133 (114)	76 (87)	67 (76)	82 (89)
M_z	6 (8)	10 (9)	11 (9)	13 (10)	121 (113)	106 (103)	90 (92)	103 (96)
z_{mm}	10 (10)	12 (12)	4 (7)	11 (10)	95 (106)	86 (103)	129 (116)	71 (83)
θ	11 (11)	14 (11)	10 (10)	9 (9)	102 (101)	108 (122)	100 (103)	77 (71)

† Acceptance region at the 5% level of significance
( ): Average value for 12 repeat tests;
Red: Outside the acceptance region.

Table 4-3 Statistical Convergence of Data (Averages for 12 repeat tests).

Var. x	Normality $\overline{X^2}$	†Confidence interval $\hat{d}$ at $N = 1{,}000$ $c = 2.0$ $\bar{x}^* - \hat{d}^*$	$\bar{x}^* + \hat{d}^*$	$c = 4.5$ $\bar{x}^* - \hat{d}^*$	$\bar{x}^* + \hat{d}^*$	E_{sc}(%) at $N = 2{,}000$ $s_x/\bar{x}$	$c = 2.0$	$c = 4.5$
U_C	471.8	1.002	1.003	1.002	1.003	0.006	0.03	0.06
β	1737.3	1.001	1.001	1.001	1.002	0.003	0.01	0.03
ϕ	139.0	0.924	0.966	0.898	0.992	0.36	1.6	3.6
F_x	60.5	0.977	1.015	0.953	1.039	0.30	1.3	3.0
F_y	72.1	0.990	1.004	0.982	1.012	0.11	0.5	1.1
M_z	119.8	0.993	1.002	0.987	1.008	0.08	0.3	0.8
z_{mm}	121.5	1.000	1.010	0.994	1.016	0.07	0.3	0.8
θ	145.5	0.959	0.997	0.936	1.020	0.25	1.1	2.5

†The cases for which the confidence interval contains the final value $\bar{x}^* = 1.0$ are colored in green, otherwise in red.

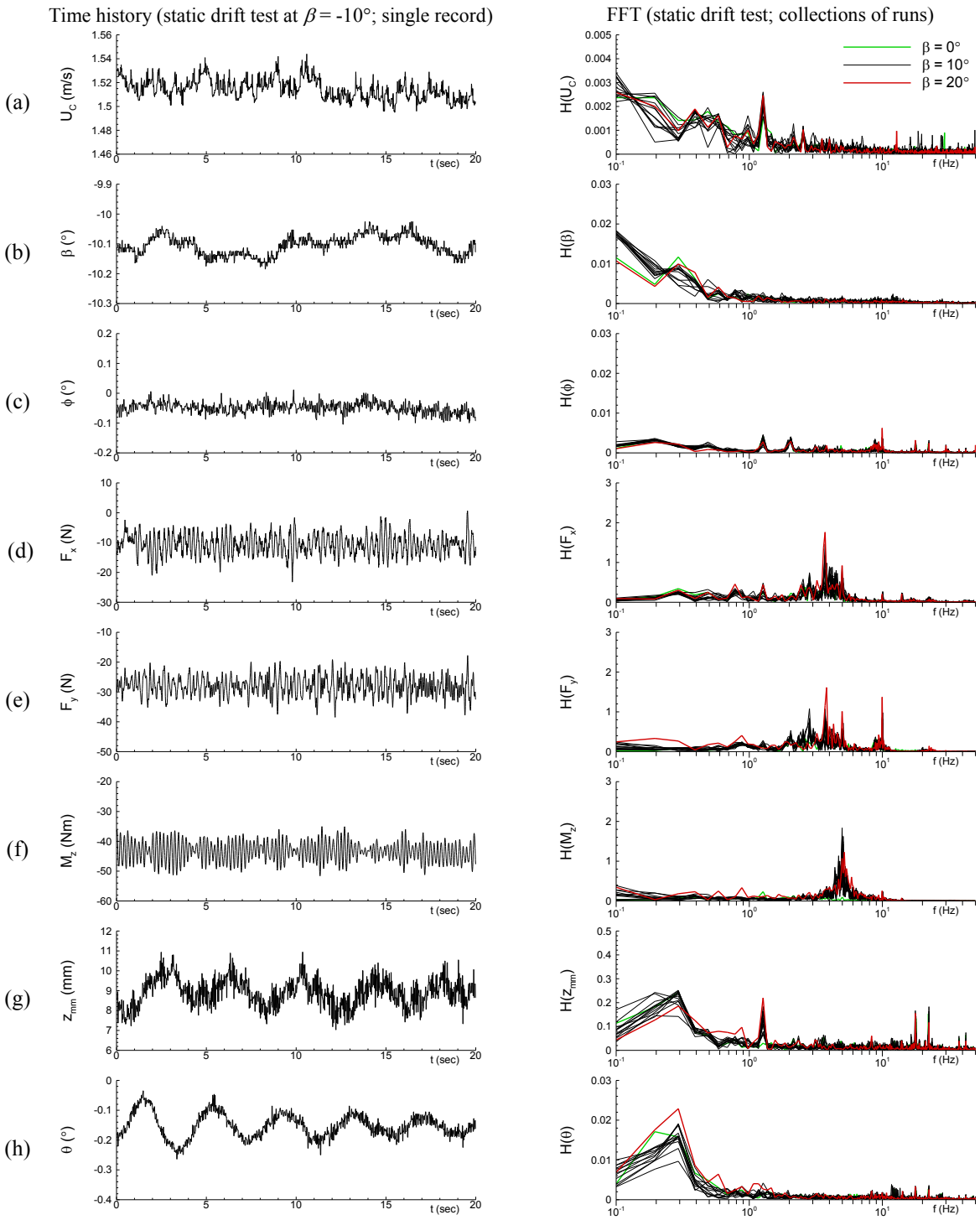

Figure 4-1 Time history (left) and FFT(right) of static drift test data: (a) U_C, (b) β, (c) ϕ, (d) F_x, (e) F_y, (f) M_z, (g) z_{mm}, and (h) θ. Tests are for $FR_{z\theta}$ mount condition and at $Fr = 0.280$.

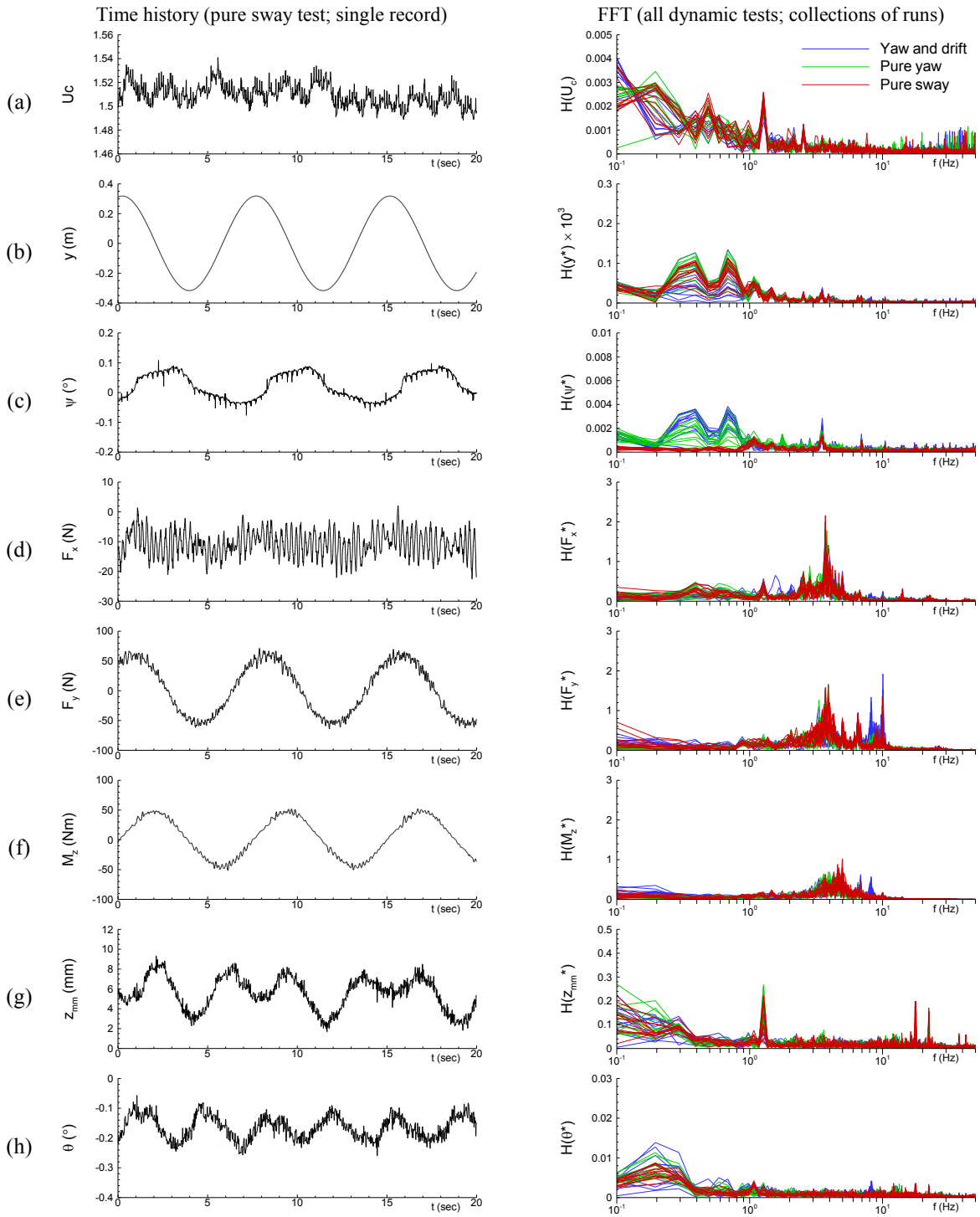

Figure 4-2 Time history (left) and FFT (right) of dynamic tests data: (a) U_C, (b) y, (c) ψ, (d) F_x, (e) F_y, (f) M_z, (g) z_{mm}, and (h) θ. Tests are for $FR_{z\theta}$ mount condition and at $Fr = 0.280$.

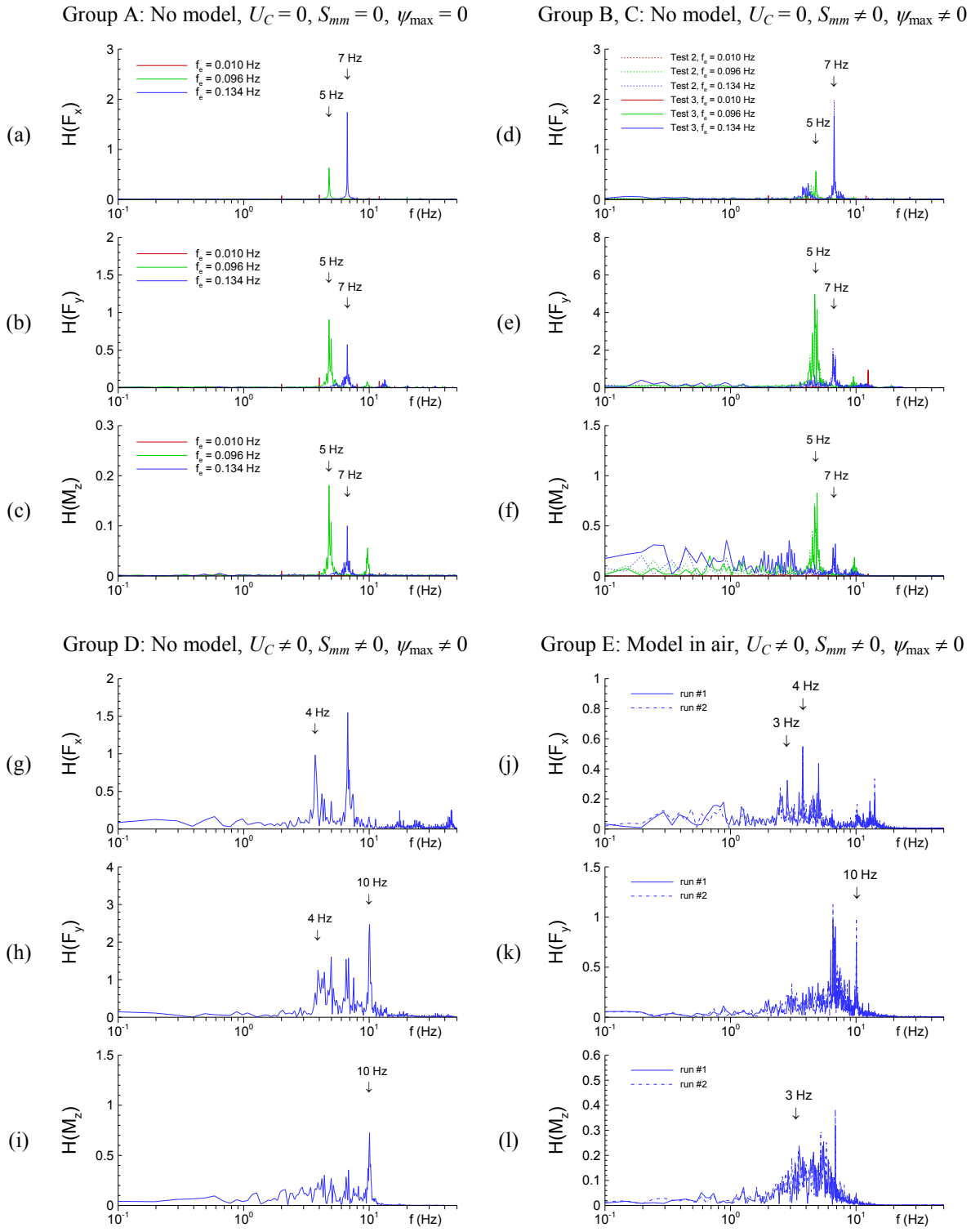

Figure 4-3 PMM noise test results: FFT for F_x, F_y, and M_z. Groups A, B, and C show noise sources for 5 and 7 Hz (natural frequencies of the load-cell) and Groups D and E for 3, 4, and 10 Hz (mechanical vibrations due to carriage speed), respectively.

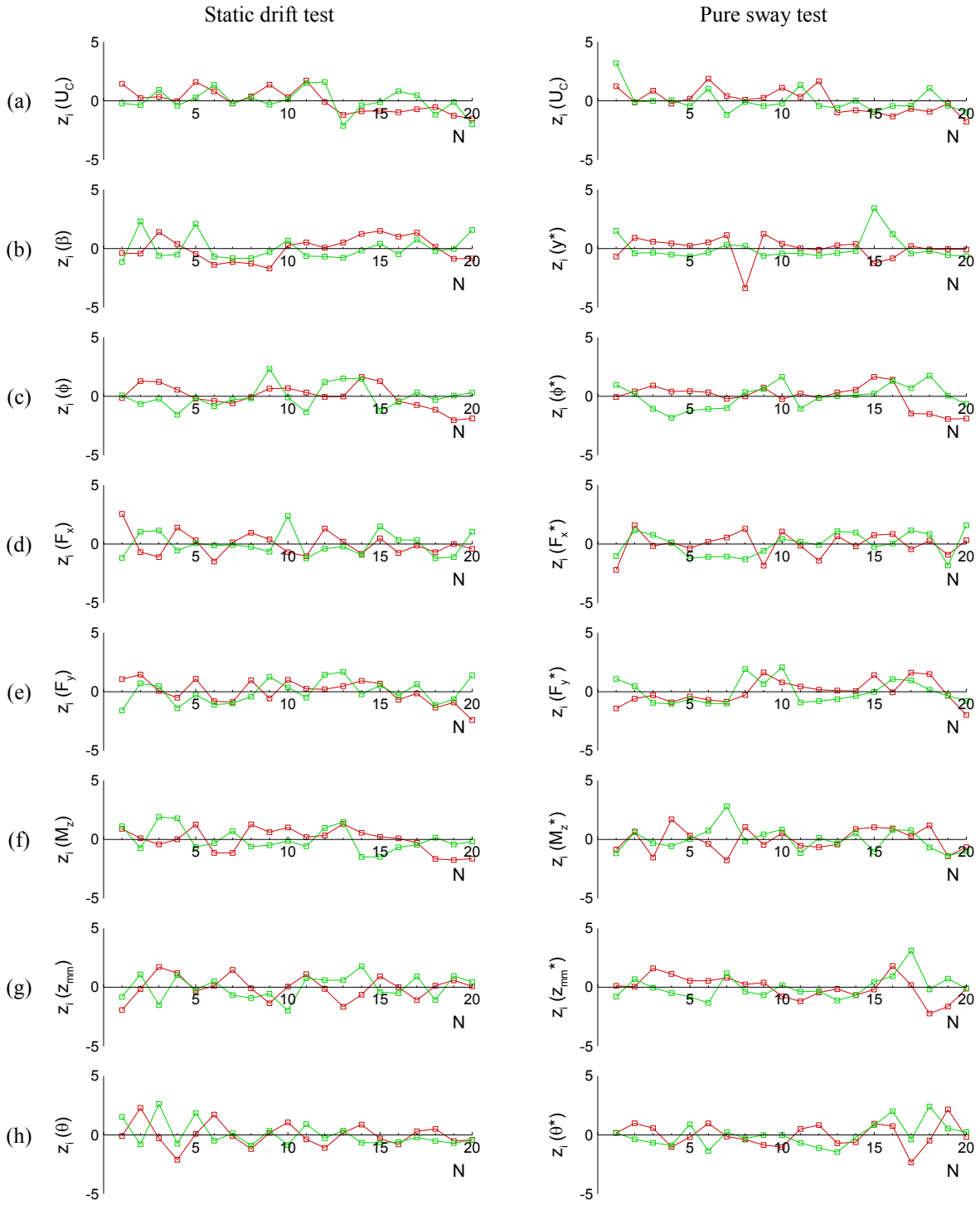

Figure 4-4 Tests for stationarity: Normalized interval mean ($\bar{x}_i$) and mean square ($\overline{x_i^2}$) values for (a) U_C, (b) β or y, (c) ϕ, (d) F_x, (e) F_y, (f) M_z, (g) z_{mm}, and (h) θ. Red: $\bar{x}_i$; green: x_i^2, which are normalized such that $z(y_i) = (y_i - m)/s$ where $y_i = \bar{x}_i$ or x_i^2 and m and s are the mean and standard deviation of y_i for $N = 20$, respectively.

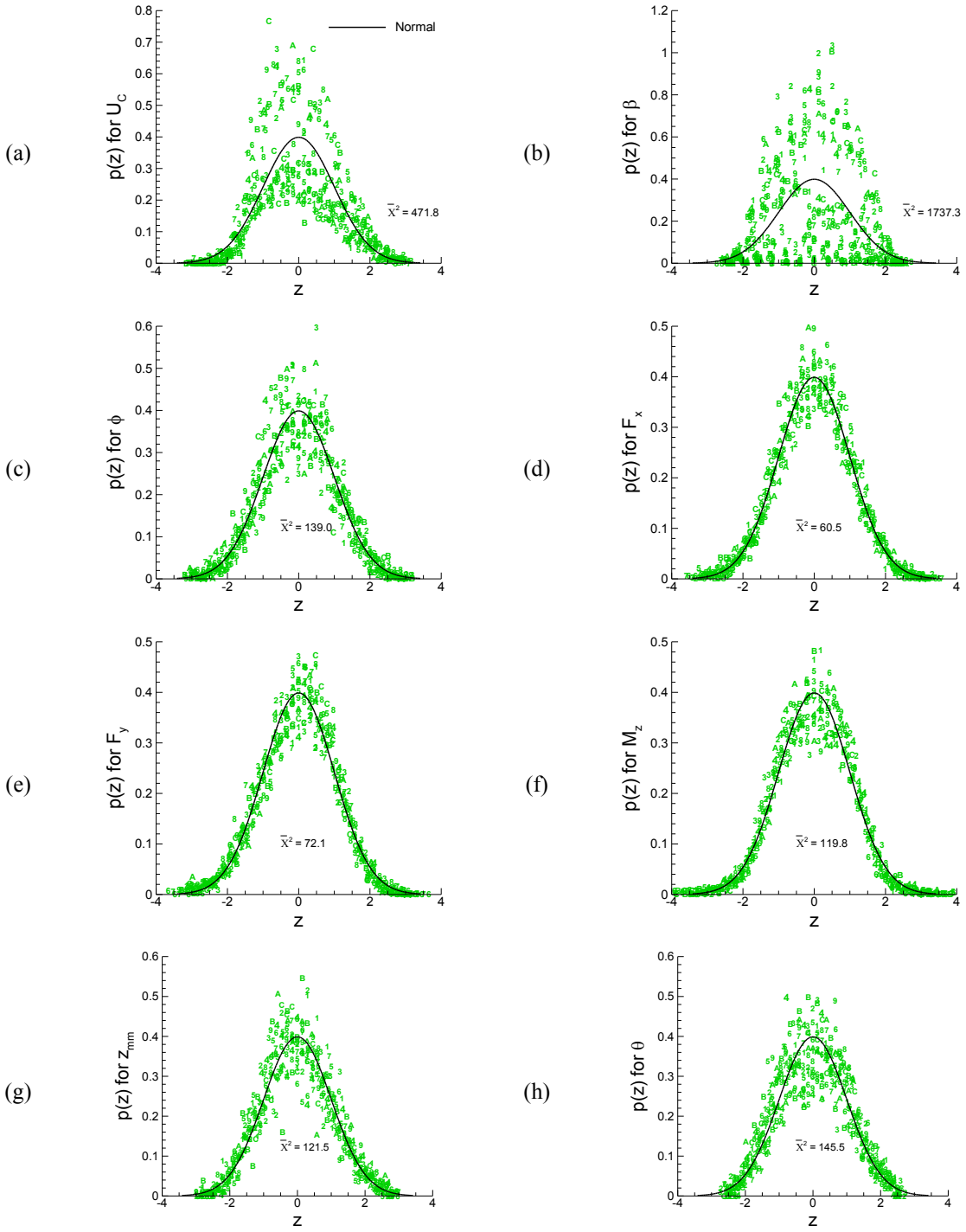

Figure 4-5 Probability density functions of the static drift test data for (a) U_C, (b) β, (c) ϕ, (d) F_x, (e) F_y, (f) M_z, (g) z_{mm}, and (h) θ, respectively. $\overline{X^2}$ is the average X^2 value of for 12 repeat tests. The acceptance region for a normality is $X^2 \leq \chi^2_{n:\alpha} = 51.0$ for $n = 36$ and $\alpha = 0.05$.

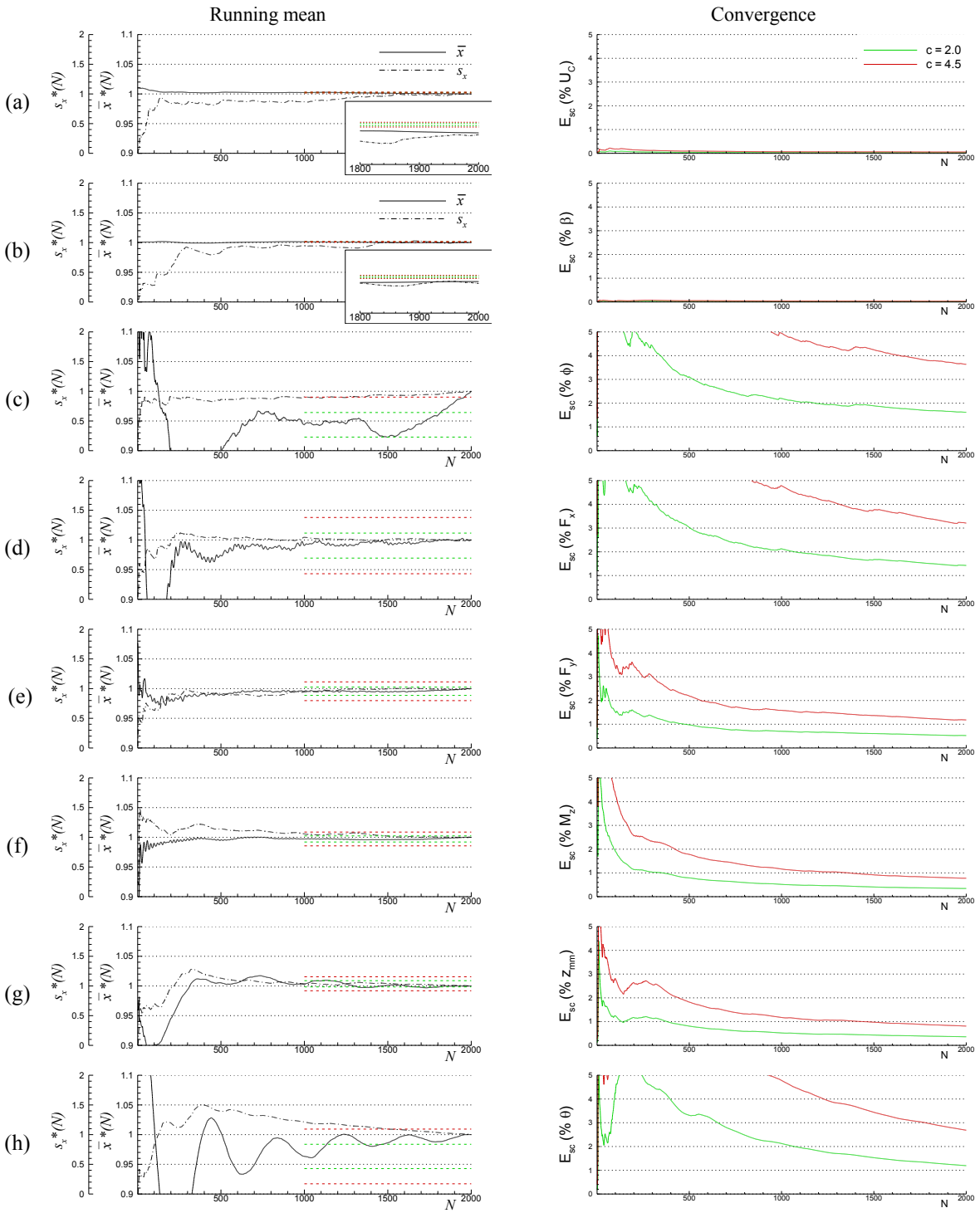

Figure 4-6 Normalized running mean $\bar{x}^*(N)$ and running standard deviation $s_x^*(N)$ (left column) and statistical convergence error E_{sc}(%) (right column) of (a) U_C, (b) β, (c) F_x, (d) F_y, (e) M_z, (f) z_{mm}, (g) θ, and (h) ϕ (Static drift test).

4.2 Phase-Averaged Flow Field Data

Statistical convergence of phase-averaged velocities (U, V, W) and Reynolds stresses (uu, vv, ww) are estimated based on the convergence of confidence interval of the variables. Let x be instantaneous velocities from N independent measurements, x at a given phase may be a stationary random variable of which statistical properties such as mean and variance values do not vary with time as the sample size N becomes large. Of interest herein is determining N where the mean and variance of the variable (i.e. the phased-averaged velocity and Reynolds stress, respectively) converge within a certain statistical confidence level, or vice versa estimating a confidence interval of the variable for a given N. For present study the confidence level are set at 95%.

The mean and variance of a sample of N independent observations from a random variable x are calculated as

$$\bar{x} = \frac{1}{N}\sum_{i=1}^{N} x_i \tag{4.14}$$

$$s^2 = \frac{1}{N-1}\sum_{i=1}^{N}(x_i - \bar{x})^2 \tag{4.15}$$

respectively. Assume x is normally distributed with a mean value of μ_x and a variance of σ_x^2. Then, the confidence interval can be established for the mean values μ_x based upon sample values $\bar{x}$ and s as follows (Bendat 1966).

$$\left[\left(\bar{x} - \frac{s \cdot t_n}{\sqrt{N}}\right) \leq \mu_x < \left(\bar{x} + \frac{s \cdot t_n}{\sqrt{N}}\right)\right] \tag{4.16}$$

where t_n is the 95% point of the Student t distribution with $n = N - 1$ degree of freedom. Which states "the true mean value μ_x falls within the noted interval with a confidence of 95%." In other words, the difference between the true and the sample mean would be

$$-\frac{st_n}{\sqrt{N}} \leq (\mu_x - \bar{x}) < \frac{st_n}{\sqrt{N}} \tag{4.17}$$

with a confidence of 95% for the sample size N. Then, the interval limit $d = st_n/\sqrt{N}$ can be used for defining the statistical convergence error for $\bar{x}$ such that

$$E \equiv \frac{d}{x_{ref}} = \frac{t_n}{\sqrt{N}} \cdot \left(\frac{s}{x_{ref}}\right) \tag{4.18}$$

indicating that the mean value of x (phase-averaged velocity) with N samples (PIV images) can has an error E of x_{ref} with a 95% confidence. Where, x_{ref} can be any reference value for x such as the phase-averaged velocities U, V, W, or the carriage towing speed U_C. From (4.18), the convergence error E is inversely proportional to the square root of sample size N and proportional to the standard deviation s of x, i.e., the turbulence intensity of the flow. If one expects a certain level of E for a mean velocity with known turbulent intensity, i.e. s/x_{ref}, then, the number of PIV images, i.e. N, can be estimated using the equation (4.18) as

$$N = \frac{4}{E^2} \cdot \left(\frac{s}{x_{ref}}\right)^2 \tag{4.19}$$

by approximating $t_n \approx 2$ for $N >> 10$.

The variance σ_x^2 for a normally distributed random variable x follows a χ^2 distribution, in contrast to the mean value μ_x following the Student t distribution as discussed above. Then, the confidence interval for the variance σ_x^2 based upon a sample variance s^2 from a sample of size N is (Bendat 1966)

$$\left[\frac{n\,s^2}{\chi^2_{n;0.025}} \leq \sigma_x^2 < \frac{n\,s^2}{\chi^2_{n;0.975}}\right] \tag{4.20}$$

where $\chi^2_{n;0.025}$ and $\chi^2_{n;0.975}$ are the 2.5% and 97.5% points, respectively, of the χ^2 distribution with $n = N - 1$ degree of freedom. Subsequently, the difference between the true variance σ_x^2 and the sample variance s^2 falls within an interval

$$-d_L \leq \sigma_x^2 - s^2 < d_U \tag{4.21}$$

with a 95% confidence, where the upper limit d_U and the lower limit d_L are

$$d_U = \frac{n\, s^2}{\chi^2_{n;0.975}} - s^2 \tag{4.22}$$

$$d_L = s^2 - \frac{n\, s^2}{\chi^2_{n;0.025}} \tag{4.23}$$

Note that as the χ^2 distribution is non-symmetric for $n > 2$, the upper and lower limits of the interval has difference values and the statistical convergence error E_U and E_L, respectively, is defined separately as follow.

$$E_U \equiv \frac{d_U}{s^2_{ref}} = \left(\frac{n}{\chi^2_{n;0.975}} - 1\right) \cdot \frac{s^2}{s^2_{ref}} \tag{4.24}$$

$$E_L \equiv \frac{d_L}{s^2_{ref}} = \left(1 - \frac{n}{\chi^2_{0.025}}\right) \cdot \frac{s^2}{s^2_{ref}} \tag{4.25}$$

where, s^2_{ref} can by any reference variance value for the random variable x such as the phase-averaged Reynolds stresses uu, vv, ww, or the turbulent kinetic energy k.

Typical examples of E, E_U, and E_L values versus the sample size N are shown in Fig. 4-7 as charts for several practical cases of the s/x_{ref} and s^2/s^2_{ref} values. The error values for an example flow field shown in Fig. 4-8 will be estimated by using the charts and the number of samples N necessary for a desired error levels. The example flow field shown in Fig. 4-8 (a) and (b) are the mean axial velocity U and the turbulent kinetic energy $k = \frac{1}{2}(uu + vv + ww)$ at the nominal wake region (x/L = 0.935) of the DTMB 5512 model in steady straight towing condition at Fr = 0.280. The mean velocity U and

the turbulent velocity fluctuations u, v, w are normalized with the model towing speed U_C = 1.531 m/s, respectively. The total number of PIV images used for the mean is N_{total} = 2,250 collected from a set of 30 carriage runs (75 images per each run). The effective number of data at the point A in Fig. 4-8 is N = 1,720 by excluding the null vectors due to insufficient PIV particle density at the point and by rejecting spurious vectors from the PIV image correlations process. Typically N is close to N_{total} at the outer flow regions and less than N_{total} inside the boundary layer or at spots where the turbulent intensity is high. At Point A, measured are the root-mean-square u = 0.09 (i.e. s of U) and the axial component of Reynolds stress uu = 0.0075 (i.e. s^2 of U), thus s/x_{ref} = 0.09 and s^2/s_{ref}^2 = 1.1 when $x_{ref} = U_C$ and s_{ref}^2 = 0.007 (the range of k), respectively, are used. From the charts in Fig. 4-7, then, the expected E for U is about 0.4% of U_C and E_U for uu is about 8% of k at $N \approx$ 1,700, respectively. For the latter case, if E_U less than 1% is desired, $N > 10^5$ is necessary. Note from Fig. 4-7 (b) that E_U is always larger than E_L and both have similar values as N increase, thus E_U can be considered as the representing E for statistical convergence of the Reynolds stresses.

The actual N = 1,720 samples of U, V, and W data measured at the point A of the previous example flow field are shown in Fig. 4-9, along with the statistics of the data and their convergence errors. The sample U_i, V_i, N_i data shown in Fig. 4-9 (a) are apparently stationary and random of which mean and variance values are $\bar{x}$ = 0.543, -0.023, 0.059, respectively, and s^2 = 0.0075, 0.0035, 0.0024, respectively. When data are normalized as $z = (x - \bar{x})/s$, all variables exhibit a standard normal distribution, shown in Fig. 4-9 (b), as assumed. The probability density functions $p(x)$ in the figure for U, V, and W are obtained by pooling the data sample into K = 35 equally spaced intervals and counting the frequency of data at each interval classes divided by N. The minimum optimum number K of class intervals was used as suggested for Chi-Square Goodness-of-Fit test (Williams 1950). Time histories of the mean values $\bar{x}$ and variance s^2 of the data using the equations (4-14) and (4-15) are shown in Fig. 4-9 (c) and (d), designated as $\bar{x}_N$

and s_N^2, respectively, as increasing the number of data sample N from 2 to 1,720. For each N, the variance s_N^2 is re-calculated using a new $\bar{x}_N$ value accounting for the newly added data sample x_N into the previous mean $\bar{x}_{N-1}$, for which the following recursive expressions are useful when N is large.

$$\bar{x}_N = \frac{1}{N}\left((N-1)\bar{x}_{N-1} + x_N\right) \tag{4.26}$$

$$s_N^2 = \left(\frac{N-2}{N-1}\right)s_{N-1}^2 + \left(\frac{N}{N-1}\right)(\bar{x}_{N-1}^2 - \bar{x}_N^2) + \left(\frac{1}{N-1}\right)(x_N^2 - \bar{x}_{N-1}^2) \tag{4.27}$$

for $N \geq 2$. As shown in Fig. 4-9 (c) and (d), the $\bar{x}_N$ converges fast for all variables typically for $N < 100$ whereas the s_N^2 first fluctuates large for $N < 500$ and converges slowly as N increases, demonstrating the stationary of the variables as assumed. Shown in Fig. 4-9 (e) are the E for U, V, W as per (4-18) and in Fig. 4-9 (f) are the E_U for uu, vv, ww as per (4-24), respectively. In the equations, the values of t_n and $\chi^2_{n;0.975}$ at each $n = N - 1$ can be found from typical textbooks on Statistics (e.g. Bendat 1966, pp. 162 and 163). The s and s^2 in the equations are evaluated by using the $\sqrt{s_N^2}$ and s_N^2 as per (4-27) at each N, respectively. Used as x_{ref} and s_{ref}^2 are the same U_C and k used at the previous paragraph. From Fig. 4-9 (e) and (f), the E and E_U exhibit similar curve shapes as those shown in Fig. 4-7 (a) and (b) at the corresponding s/x_{ref} (0.09, 0.06, 0.05 for U, V, W, respectively) and s^2/s_{ref}^2 (1.1, 0.5, 0.4 for uu, vv, ww, respectively), respectively. From Fig. 4-9 (e) and (f), at N = 1720, E = 0.4% for U and E_U = 8% for uu are the same as the chart readings from Fig. 4-7 (a) and (b), respectively, proving the validity of the method. The E's for V and W are smaller than for U, about 0.3%, respectively, and the E_U's for vv and ww are also smaller than for uu, 4% and 3%, respectively, as well agree with the chart readings.

The application of the method to phase-averaged PMM PIV measurement is shown in Fig. 19. Shown in the figure are the phased-averaged (a) mean axial velocity U and (b) turbulent kinetic energy k of the same model for the previous example case but in

a forced dynamic pure yaw motion. The measurement location is at the same x/L = 0.935 as for previous example flow case, whereas shifted in lateral direction more to the starboard side of the model. Selected for a presentation case out of the 32 phase groups of the PMM PIV measurements is the 180° case where the flow structure is largest at the port side thus slower convergences (larger convergence error) of the mean flow variable values are expected. Total 100 carriage runs were made to sample N_{total} = 250 PIV images collected from 2.5 PMM cycles per each run. As shown in Fig. 4-10, the flow field becomes more complex than the steady towing case shown in Fig. 4-8 due to the forced oscillatory PMM motions of the model, accordingly stronger turbulence of the flow with about two times larger range of turbulent kinetic energy, $[k]$ = 0.014. To see more global trend of the convergence, the flow field points are grouped into three categories: Group A ($0 < k/[k] \leq 0.1$), Group B ($0.1 < k/[k] \leq 0.5$), and Group C ($0.5 < k/[k] \leq 1.0$), representing the regions where fast, moderate, and slow convergence is expected, respectively. In Table 4-4, presented are the ranges and average values of the effective number of PIV images N, turbulence intensity $\sqrt{k}$ (approximately corresponds to the average of u, v, and w), the normalized turbulent kinetic energy $k/[k]$, and the convergence errors E and E_U for the Groups A, B, and C, respectively. The average effective PIV image numbers N = 235, 210, and 177 respectively for each group corresponds to 94%, 84%, 71% of N_{total}, respectively, due to the same reasons as explained previously for the steady flow case. The $\sqrt{k}$ and $k/[k]$ correspond to the statistical convergence parameters s/x_{ref} and s^2/s_{ref}^2, respectively, which can be used for the chart (Fig. 4-7) readings along with N estimating the convergence errors. The ranges and average values of E and E_U presented in the table are for all phase-averaged mean velocities U, V, W and Reynolds stresses uu, vv, ww, respectively. In spite of relatively smaller sample number, N ~ 200 (for the steady towing case N ~ 2,000), E for the mean velocities is usually smaller than 1% of U_C, at best about 2% for Group C, and E_U for the mean Reynolds stresses is also satisfactory less than 10% of $[k]$ in average. However, E_U can be significantly large

up to 36% at the region where $k/[k] \approx 1.0$ (upper left corner of Fig. 4-10) and the number of PIV images required to reduce E_U to 10% is $N \sim 1{,}000$ from Fig. 4-7, which requires more than 400 times of carriage runs.

From the above two example flow cases, it is shown that the statistical convergence of PIV measured mean velocities and Reynolds stresses can be estimated using the confidence intervals of the mean and variance values by assuming those variables are stationary and random following the normal distribution. From the first example flow, steady straight towing condition, where a large number of data ($N \sim 2{,}000$) is available, revealed that the instantaneous velocity data are stationary random variables following a normal distribution as assumed and accordingly their mean values follow Student t distribution and variance values χ^2 distribution. From the second example flow, forced oscillatory PMM motions, even with relatively small number of data ($N \sim 200$), statistical convergence errors E and E_U values are fairly small, usually less than 1% of U_C and 10% of $[k]$, for the phase-averaged velocities and Reynolds stresses, respectively. Those statistical convergence errors indicate that the true mean and variance values may differ from the sample mean and variance values by the amount of E and E_U, respectively, with a 95% confidence. However, the term 'true mean' should be distinguished from the term 'true value' as the former value may biased from the latter value, if exists, due to systematic errors which can be identified by calibrating the PIV system to a known standard. In the uncertainty analysis (UA) contexture, then, the convergence error can be considered as the precision limit at the '1st-order replication-level' (Coleman and Steel 1999 and Moffat 1982, 1985, and 1988) as all the PIV system remain the same as sample after sample is tested. Thus the 'true value' relative to the measurement values can be estimated at the '*N*th-order replication-level' including the random errors together with the systematic errors, which will be further discussed at the Section 4 'Uncertainty Analysis'. Lastly, estimating the '1st-order replication-level' precision limits of the mean Reynolds stresses, it should be noted that the typical UA procedures (assuming Student t distribu-

tion of data) can underestimate the precision limit significantly as the Reynolds stress data actually follow the χ^2 distribution which converges much slower than the Student t distribution.

Table 4-4 Statistical convergence of Phase-averaged velocity and Reynolds stress.

Group	A	B	C
N	62 ~ 251 (235)	106 ~ 243 (210)	107 ~ 232 (177)
$\sqrt{k}$	0.02 ~ 0.04 (0.03)	0.04 ~ 0.08 (0.06)	0.08 ~ 0.12 (0.09)
$k/[k]$	0.02 ~ 0.1 (0.06)	0.1 ~ 0.5 (0.25)	0.5 ~ 1.0 (0.62)
E (% U_C)	0.1 ~ 0.8 (0.3)	0.2 ~ 1.4 (0.6)	0.5 ~ 2.4 (1.1)
E_U (% $[k]$)	0.1 ~ 3.5 (0.9)	0.5 ~ 15.0 (3.8)	2.3 ~ 35.9 (10.4)

( ) : average value; $[k]$ is the range of k.

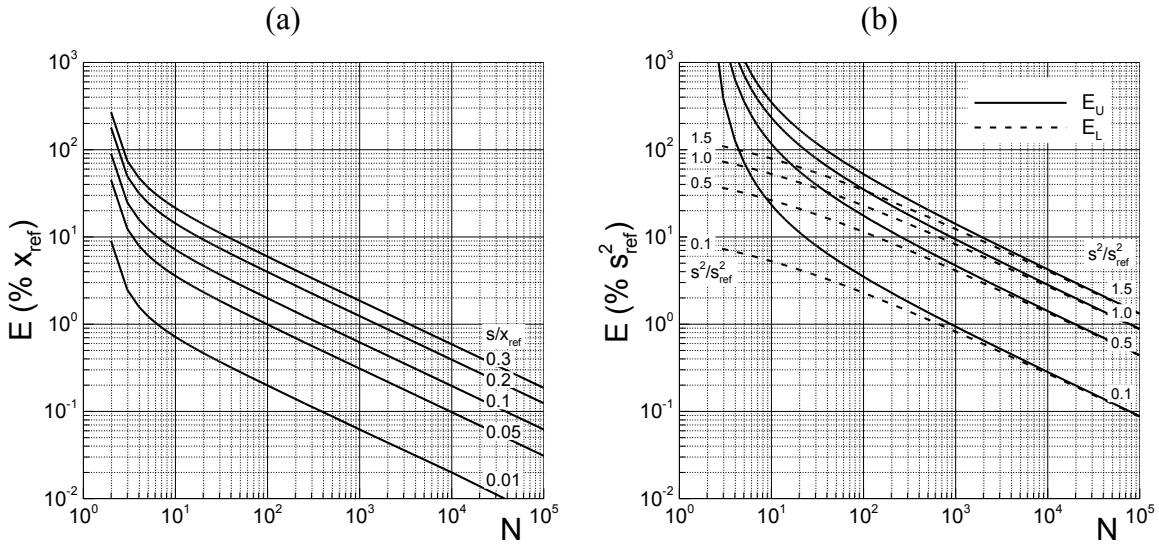

Figure 4-7 Statistical convergence errors of (a) the mean $\bar{x}$ and (b) variance s^2 for stationary random variable x.

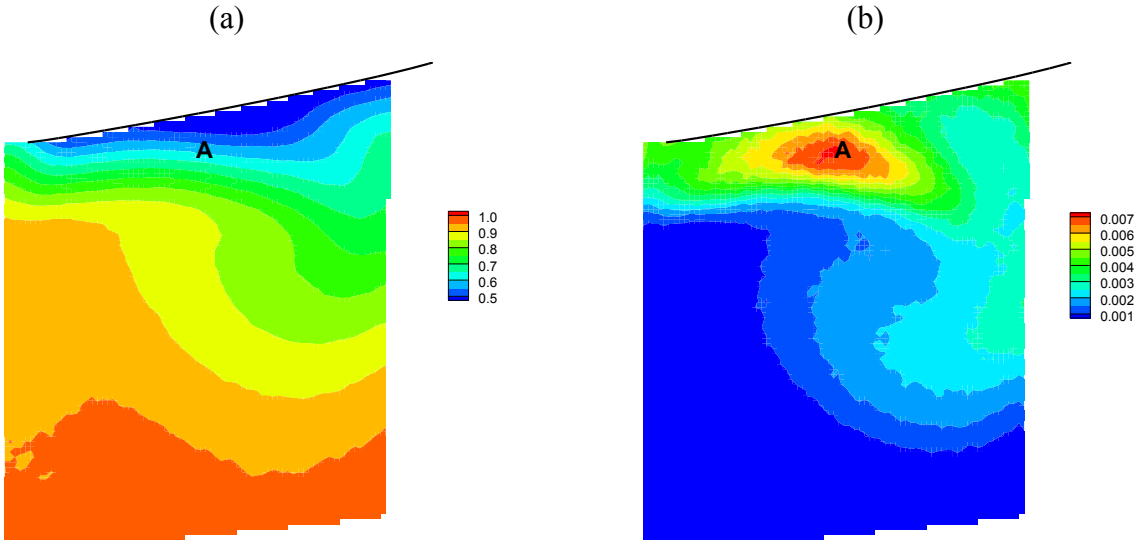

Figure 4-8 Example PIV flow field data: Contours of (a) mean axial velocity U and (b) mean turbulent kinetic energy k of DTMB 5512 model in steady straight towing at Fr = 0.280 condition. Measurement location is at x/L = 0.935, near the center plane of the model (port side). The total number of PIV images used for averaging N_{total} = 2,250 and the effective number N = 1,720 at Point A.

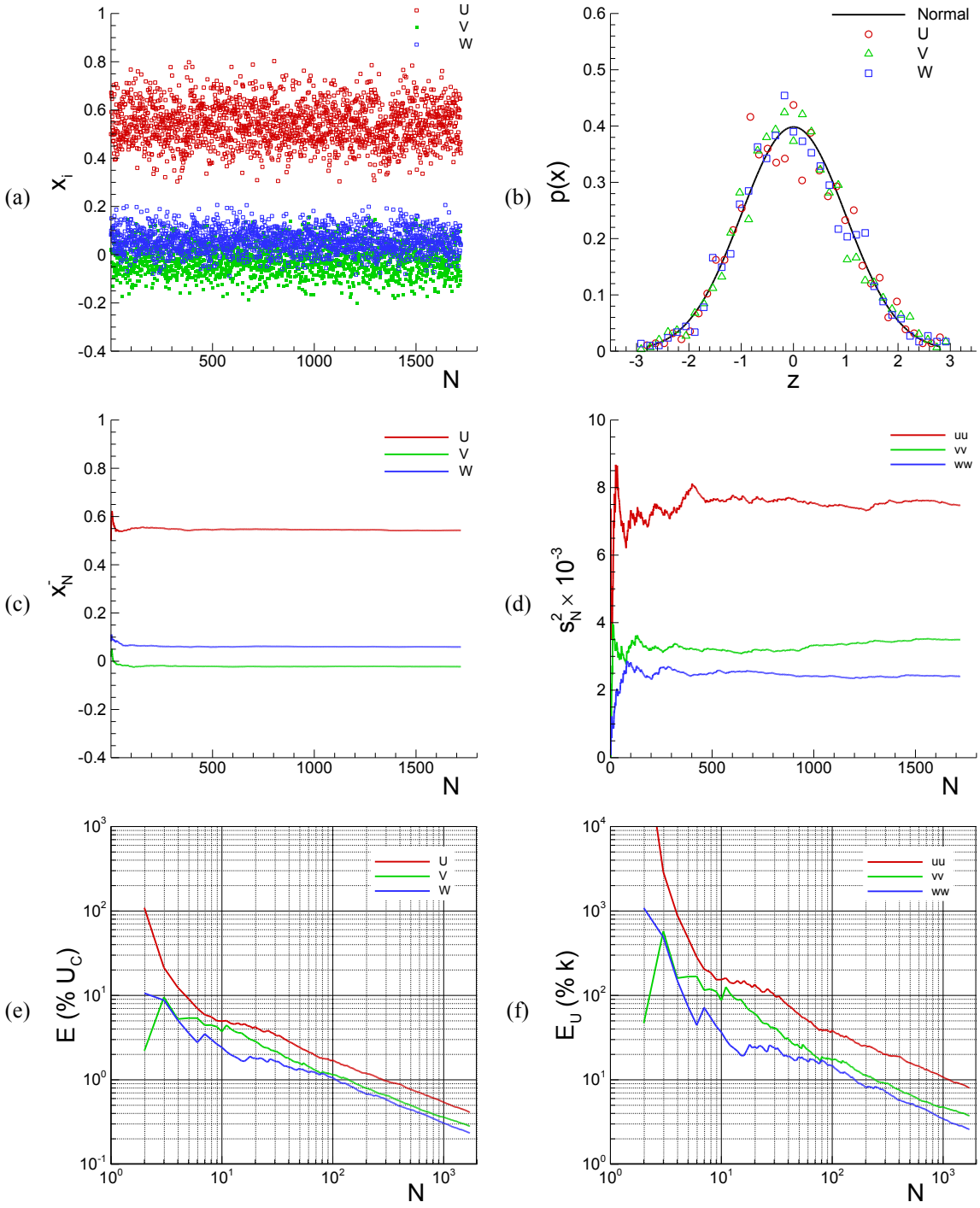

Figure 4-9 Flow data and statistics for Point A of the example flow: (a) instantaneous velocities U_i, V_i, W_i, (b) standard normal probability density function $p(x)$, (c) running mean $\bar{x}_N$, (d) running variance s_N^2, (e) E for U, V, W, and (f) E_U for uu, vv, ww, respectively.

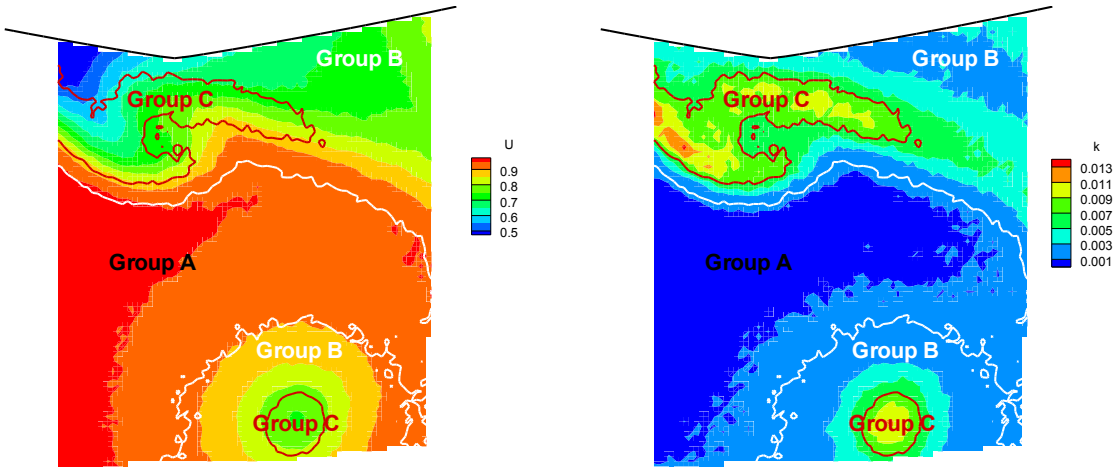

Figure 4-10 Example PMM PIV flow field data: Contours of phase-averaged (left) axial velocity U and (right) turbulent kinetic energy k of DTMB 5512 model in pure yaw motion ($\gamma = 180°$) at $Fr = 0.280$. Measurement location is at $x/L = 0.935$, near the keel of the model. The total number of PIV images $N_{total} = 254$.